Heat-to-Connect: Surface Commensurability Directs Organometallic One-Dimensional Self-Assembly

Felix Hanke,[†,*] Sam Haq,[†] Rasmita Raval,[†,*] and Mats Persson[†,‡]

[†]Surface Science Research Centre and Department of Chemistry, University of Liverpool, Liverpool, L69 3BX, United Kingdom, and [‡]Department of Applied Physics, Chalmers University of Technology, SE-412 96, Göteborg, Sweden

ABSTRACT

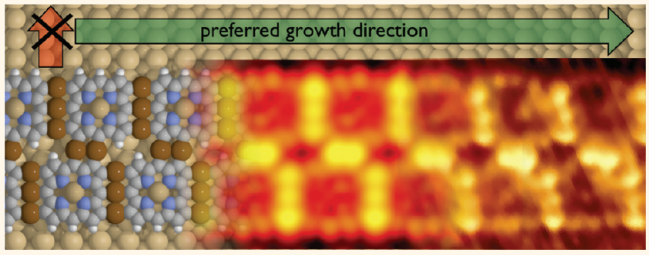

Recent experiments demonstrated the assembly of unfunctionalized porphyrin molecules into organometallic wires on the Cu(110) surface through the formation of stable C—Cu—C bonds involving Cu adatoms. The remarkable property of the observed structures is that they adopt a clear direction, despite the lack of functional ligands to direct the assembly. Here we use density functional theory calculations and scanning tunneling microscopy to clarify the mechanism for the highly one-dimensional assembly of the observed nanostructures. An energetic preference for the formation of C—Cu—C bonds is found in several lattice directions, but self-assembly critically relies on the commensurability of appropriate adsorption sites for the Cu atoms involved in the coupling. The experimentally observed structures arise from a geometric self-limitation of the assembly process, which proceeds in the energetically and geometrically most preferred direction. A further extension of the structure in the orthogonal dimension to form 2D assemblies is prevented by the lattice mismatch between the repeat lengths in the ⟨001⟩ and ⟨110⟩ directions of the underlying (110) lattice and the apparent rigidity of the molecules involved. However, the fusing of two parallel chains is geometrically allowed and leads to some of the energetically most favorable configurations. Finally, the role of van der Waals forces is investigated for the covalent couplings and chemisorbed interactions found in this system.

KEYWORDS: covalent self-assembly · porphyrins · substrate commensurability · van der Waals forces · density functional theory (DFT) · scanning tunneling microscopy (STM)

The functionalization of surfaces *via* molecular assembly is a highly promising avenue toward the design of nanoscale properties,[1−3] such as nanopores in molecular networks,[4−7] nanowires,[8,9] or nanoribbons.[10,11] For each functionalization, the atomic-scale understanding and control of all processes involved is essential. To date, almost every type of intermolecular interaction has been used as a driving force to create ordered adsorbate structures. Reports in the literature range from utilizing very weak van der Waals forces between adsorbed molecules[12−14] and slightly more stable hydrogen bonds[2,15−18] to fully covalent bonds for on-surface self-assembly.[1,10,11,19−22] A rapidly growing class of systems is based on metal-coordination bonds,[3] where substrate atoms form covalent bonds with the adsorbates. Several distinct approaches to create metal-coordination based nanostructures have been pursued, which are generally based on molecular modules containing cyano, pyridyl, or other electron donating functional groups.[23−29] The resulting couplings almost exclusively involve N—Cu bonds. However, the dehalogenation of C—Br functionalized molecules on Cu(111) has also been shown to yield covalent C—Cu—C bonds as well.[30]

All of these systems require the presence of specific and often interlocking functional groups to achieve the assembly of a desired structure. Could the restrictions imposed by such functionalizations be overcome by using the underlying surface structure instead?

Haq *et al.*[31] recently demonstrated how this could be achieved with completely unfunctionalized porphyrin cores adsorbed on Cu(110), which were subsequently heated to several hundred Celsius. In a *heat-to-connect* assembly strategy, the surface was used as the only means to activate, connect, and direct the self-assembly into one-5dimensional chains that are coupled by organometallic C—Cu—C bonds. For *unsubstituted* Cu—porphyrin molecules, extended two-dimensional assembly was never observed, but parallel chains could sometimes bond together, which suggests the existence of a

* Address correspondence to hanke@liverpool.ac.uk, raval@liverpool.ac.uk.

Received for review August 30, 2011 and accepted October 17, 2011.

Published online October 17, 2011
10.1021/nn203337v

© 2011 American Chemical Society

chemical and energetic driving force toward a fully two-dimensional self-assembly. However, this process appears to be self-limiting, as never more than two to three parallel coupled chains have been observed. This system, therefore, poses the intriguing question: how is such a well-defined one-dimensional assembly achieved in a system that does not have an obvious growth direction?

This is particularly important as subtle and nonobvious changes in the physical conditions can lead to changes even in the dimensionality of the adsorbate structures.[18] The potential applications for a successfully controlled surface/adsorbate structure are many and include for example molecular[32] and spin storage arrays[33] for two-dimensional systems to connecting molecular wires[8,9] for 1D-self-assembly. An outstanding problem for the control and prediction of adsorbate nanostructures is to work out the physical principles governing the dimensional and directional control for adsorbate molecules. This task is relatively easy in cases where there are obvious symmetry constraints, or where the molecule has been specifically functionalized. However, for a symmetric molecule lacking well-defined coupling points, achieving directional control is much more challenging.[1] In particular for engineering heterogeneous nanostructures consisting of multiple adsorbates and different functionalities, it is vital to understand all relevant mechanisms that affect the adsorbate structure.

Here we clarify the mechanisms responsible for the self-assembly and apparent self-limitation of the two-dimensional self-assembly for the Cu−porphyrin chains described by Haq *et al.*[31] To this end, scanning tunneling microscopy (STM) was combined with large-scale density functional calculations and STM simulations, carried out for a catalogue of adsorption and coupling geometries that span the full range of conceivable directions and orientations for the coupled porphyrin geometries. It is shown in detail how the Cu(110) substrate provides the templating that facilitates the self-assembly in one dimension despite the complete lack of specific functionalization in the porphyrin core. For the creation of strongly coupled nanostructures, Cu surfaces stand out as they are very likely to form metal-coordination bonds with a variety of molecular systems and apparently also form covalent bonds with organic adsorbates. In contrast with other coinage metals, the copper surfaces have a higher reactivity. Along with the availability of free adatoms well below the desorption and sublimation temperatures of large molecular adsorbates, they provide the optimal combination for the formation of structured networks. This combination is due to the comparatively high-lying *d*-states in the Cu band structure, coupled to its relatively low cohesive energy.[34]

RESULTS AND DISCUSSION

Porphyrin Self-Assembly on Cu(110). In this work, we focus on the unfunctionalized Cu−porphyrin molecule, whose structure is given in the inset of Figure 1a. The adsorption of porphyrins on Cu(110) has been studied in detail,[31,35,36] and the nature of the interaction between porphyrins and the Cu surface has been well established. The π-orbitals of the porphyrin macrocycle hybridize with the *sp*-band and the *d*-states of the Cu(110) surface in a covalent molecule-surface bond, with the metalated center of the molecule being located on a short-bridge site on top of the Cu rows. Upon heating, the macrocycle is able to capture Cu adatoms that originate from step edges.[36] These captures eventually lead to the activation of the C−H bonds and the subsequent formation of the porphyrin chains. Furthermore, the chemical nature of the coupling between adjacent macrocycles is consistent with an organometallic bond involving C−Cu−C linkages.

The effect of thermal annealing is illustrated in Figure 1. After adsorption at room temperature, the porphyrin macrocycles form islands that are stabilized by adatoms captured between the molecules, Figure 1a.[36] Upon heating to 300−330 °C, the molecules couple covalently to form distinct motifs with different coupling configurations, Figure 1b.[31] Note the three different directions in which the coupling can proceed initially. The main self-assembly direction is perpendicular to the ⟨100⟩-rows of the Cu surface, but partially annealed systems have also been observed which couple by 13° and 25° off this direction, corresponding to a porphyrin molecule that is offset by one or two lattice spacings along the Cu rows, respectively. The next stage of the annealing process produces extended linear ribbons, where the individual porphyrins are connected in the ⟨100⟩ direction, for example, perpendicular to the Cu rows, with either two or three adatoms, Figure 1 (c). Further heating can lead to the fusion of two parallel coupled Cu-porphyrin chains as the last stage before dissociation of the molecules, Figure 1d.

In the light of these observations, it is particularly important to investigate how the assembly is controlled in this self-assembly phenomenon. From the images presented in Figure 1, three possibilities for the growth mode come to mind. First, the assembly could be completely randomly directed. Some evidence for this arbitrary coupling is seen in Figure 1b, where multiple different couplings are observed for a partially annealed system. However, by the end of the self-assembly process, the chains are perfectly straight over several tens of nanometers. The second possibility, then, is that of a preferred one-dimensional self-assembly which is supported by our experimental observations. Third, the nature of the fused porphyrin

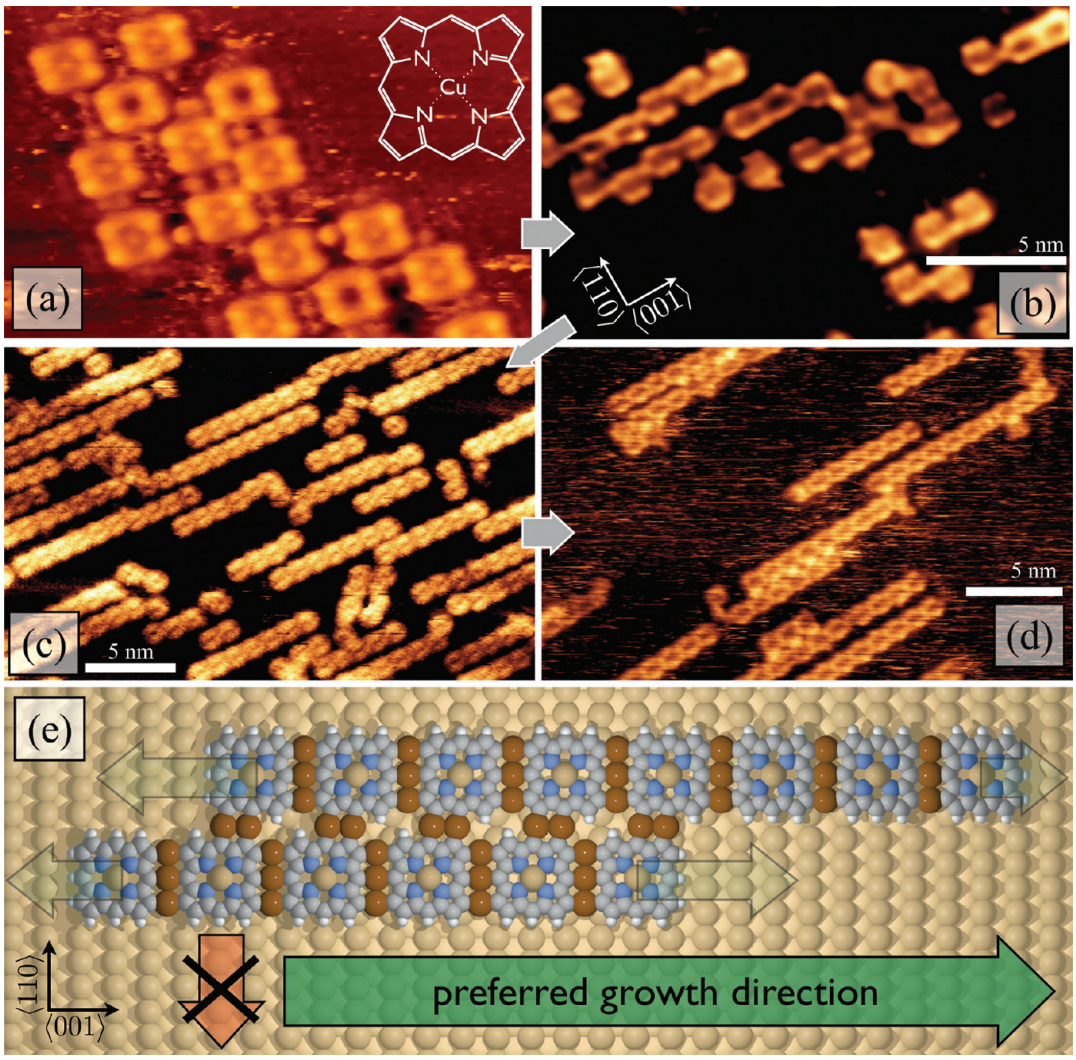

Figure 1. Formation of covalently bonded porphyrin chains on Cu(110): (a) Cu−porphyrins adsorbed on the Cu(110) surface at low coverage and room temperature form islands and capture Cu adatoms. The inset shows the molecular structure of the metalated porphyrin core. (b) C−Cu−C coupling is initiated when the surface is heated to a temperature of 300−330 °C, where different intermediate states involving one or two connecting Cu atoms is observed. Note in particular how neighboring macrocycles can be offset in different lattice directions. (c) The formation of porphyrin chains, one macrocycle wide, is observed upon annealing at ∼375 °C, (d) The fully annealed (at 400 °C) surface sometimes forms oriented porphyrin chains, where no more than two chains connect in parallel. The porphyrin centers in the parallel chains are offset by a single lattice spacing in the ⟨001⟩ direction. (e) Model representation for the central chain in panel d, showing the orientation on the Cu(110) surface rows and the growth direction with a green arrow. The red arrow denotes the direction in which no further growth is seen.

chains and its growth mode requires investigation. This chain coalescence provides evidence of a driving force toward full 2D assembly, but the nature of this driving force and particularly the origin of any restrictions placed on the structures remain to be clarified.

Energetics of the C−Cu−C Couplings. Periodic density functional theory (DFT) in the generalized gradient approximation (GGA)[37−39] has been used to explore the organization of the observed chains. The binding energy of a porphyrin macrocycle is calculated for each of the possible couplings configurations that could potentially be consistent with the observations discussed above. Scheme 1 labels the main couplings considered in this study in terms of the number and location of the connecting Cu adatoms, which could in principle occur in any surface direction, and in a variety of combinations for a two-dimensional overlayer. The label for each configuration denotes the number of connecting Cu adatoms (**0** to **3**) and the type of coupling in a single lattice direction, indicated by the letters **s** (symmetric), **as** (asymmetric), and **off** (offset). The overall binding energies for all computed configurations are presented in Figure 2. These results are displayed in three groups, corresponding to self-assembly perpendicular to the Cu rows (a), parallel to the Cu rows (b), and for full 2D assembly (c). Figure 2a contains the results obtained in ref 31 along with a number of additional structures that are observed for partially annealed systems.

Coupling Perpendicular to the Cu Rows: The ⟨001⟩ Surface Direction. A clear trend is visible for the self-assembly perpendicular to the Cu rows, whereby the binding energy increases with each additional Cu coupling, and where the lowest-energy structure is either in configuration **2s** or **3**. As demonstrated in Figure 1, the self-assembly in the ⟨001⟩-direction begins with single C–Cu–C linkages and follows the energy hierarchy calculated in Figure 2a. In the initial stages, two adjacent porphyrin molecules can be offset by one or two lattice spacings along the ⟨110⟩-rows and still be linked with one intermediate Cu atom. These correspond to mixtures of symmetric and asymmetric configurations **1s** and **1as**. Interestingly, the binding energy for these mixed offset couplings can be well described with an average binding energy for the two couplings that form the offset. The equivalent offset configuration for two coupling Cu adatoms, **2off**, was observed exceptionally rarely in STM images on partially annealed systems. This observation agrees with the computed result that the **2off** configuration is energetically less favorable than either of the straight couplings **2s** or **2as** which are seen frequently.

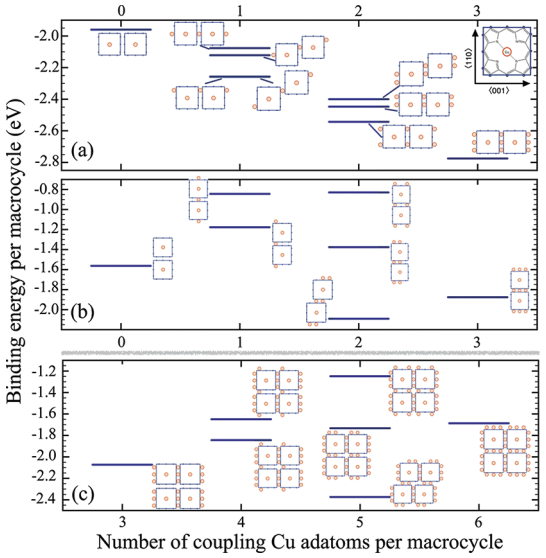

Figure 2. Binding energies per porphyrin core for different self-assembled periodic structures: (a) perpendicular to the Cu rows (⟨001⟩ surface direction), (b) parallel to the Cu rows (⟨110⟩ surface directions) and (c) for a full 2D overlayer. See text for a detailed discussion.

Coupling Parallel to the Cu Rows: The ⟨110⟩ Surface Direction. The picture changes significantly when considering self-assembly in the ⟨110⟩ direction, parallel to the Cu rows and perpendicular to the observed chains, as presented in Figure 2b. It is still energetically favorable to couple porphyrins into chains *via* C–Cu–C bonds, but the hierarchy that more Cu coupling atoms correspond to a higher stability is broken. In fact, there are only two stable configurations compared to the uncoupled porphyrin rings, these are of type **2off** and **3**. However, the lowest binding energy found for these chains is −2.09 eV, which is far from being competitive with any of the coupling configurations parallel to the Cu rows discussed above.

The Two-Dimensional Adlayer. The trend observed for the ⟨110⟩ couplings persists when analyzing fully two-dimensional self-assembly, shown in Figure 2c. The couplings considered all have the triply connected type **3** connection perpendicular to the Cu rows as observed experimentally, but include all possible couplings in the orthogonal direction. Again, the only configuration that is more stable than the uncoupled parallel chains involves one type **3** and one type **2off** coupling per macrocycle, which we label as $(\mathbf{3/3})_{2D}$ and $(\mathbf{3/2off})_{2D}$ respectively. The "2D" denotes the full 2D overlayer. Interestingly, only these two couplings are observed when the fused porphyrin chains are created.

According to the results presented in this section, self-assembly is highly preferred perpendicular to the Cu rows. The highest possible binding energy per macrocycle occurs in the final assembly step as shown in Figure 2a. This discussion also provides detailed computational evidence based on energetics that two-dimensional self-assembly is strongly hindered, as a direct consequence that one-dimensional assembly is much more favorable. We now turn to some of

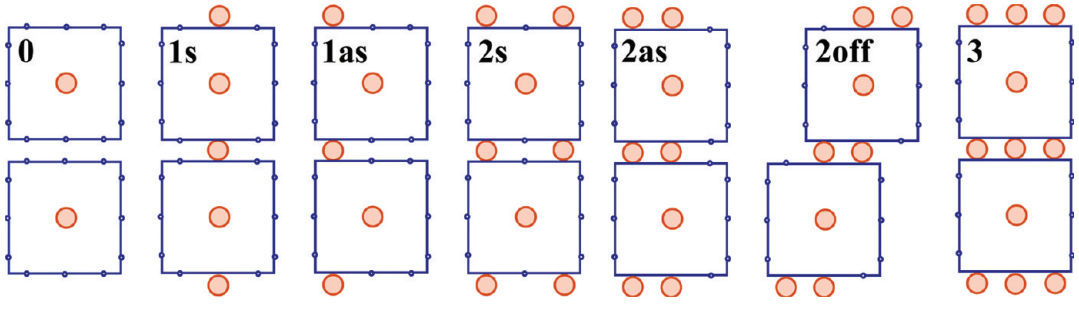

Scheme 1. Periodic configurations for the C–Cu–C couplings of porphyrin molecules in one dimension. Each square represents one porphyrin molecule. In principle, each of these connections could be possible in two lattice directions along and perpendicular to the Cu rows although not all of the possible structures shown have been observed experimentally. The label in the top left corner of each image denotes the number of coupling Cu adatoms and their position, *e.g.*, symmetric (s), asymmetric (as), or offset (off). These labels are used throughout this work

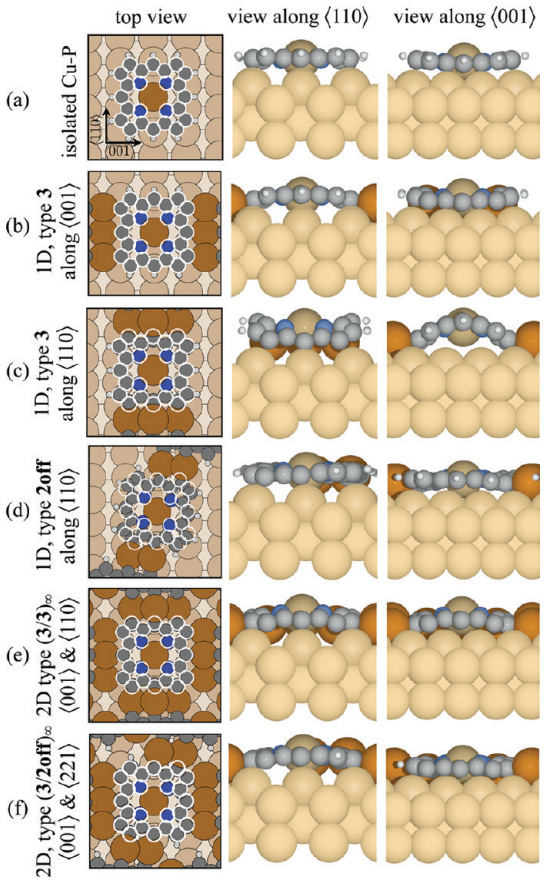

Figure 3. Optimized molecular structures for different directions of self-assembly on the Cu(110) surface in one and two dimensions. For each structure, the top view (left) schematically shows the position of each atom in the porphyrin core. The white circles correspond to the porphyrin core of the unperturbed (top row) structure, and demonstrate the degree of horizontal distortion. The middle and right views are taken parallel and perpendicular to the Cu rows respectively and demonstrate the vertical buckling of the structures.

the geometric properties of the structures so as to explain the obtained energetic hierarchies.

Role of the Surface Geometry. *Perpendicular to the Cu Rows: The ⟨001⟩ Surface Direction.* The relaxed molecular structures for a number of representative coupling configurations from Figure 2 are presented in Figure 3. The configurations chosen are the most stable couplings in each of the different lattice directions. To illustrate the role of the surface geometry, we show a schematic top view of the structure and views along the two main lattice directions of the Cu(110) surface. The top row in Figure 3 contains the structure of an adsorbed Cu−P molecule without coordination bonds and is used as a reference. To facilitate the comparison across different surfaces, white circles have been used to label the position of the atoms in the reference structure and are plotted in identical positions on each image of the left column of Figure 3.

Figure 3b denotes the most stable structure for self-assembly perpendicular to the Cu rows.[31] From the white circles on that structure (representing the uncoupled configuration **0** in an equivalent position), and by comparing the two side views to the reference porphyrin, one can see that the porphyrin core has virtually no distortion in this configuration. This lack of distortion is a primary driver for porphyrins to covalently couple in the ⟨001⟩ direction: each C−Cu−C bond provides additional chemical stability, while the surface geometry (and hence the nature of the chemisorption bond) remain unchanged.

Parallel to the Cu Rows: The ⟨110⟩ Surface Direction. The situation changes considerably when we look at the two most stable configurations for self-assembly parallel to the Cu rows. For type **3** coupling in this direction, the comparison between actual atomic positions and those of the free adsorbed macrocycle in the top view in Figure 3c,d already hints at a very strong distortion of the porphyrin molecule. The two side views also show a strong vertical buckling, which amounts to 1.41 Å, as measured by the height difference between the highest and lowest C or N atoms. This buckling is much larger than the 0.49 Å found for the type **3** coupling in the ⟨001⟩-direction or the corresponding height difference of 0.34 Å for a single adsorbed Cu−P molecule. Interestingly, the vertical height difference of the **2off** configuration (0.39 Å) in the ⟨110⟩ direction is almost the same as in the original type-**3** coupling. The **2off** coupling is offset by one lattice spacing perpendicular to the Cu rows (see Figure 3d) and allows extra space for the porphyrin to relax by rotating in the surface plane through 6.3° from its original orientation and is actually the most stable of the configurations in the ⟨110⟩ direction. Type **2off** coupling is also observed experimentally as the primary linkage between two parallel coalesced porphyrin chains.

2D Assembly. We now turn to the hypothetical full 2D overlayer, for which two configurations are presented in the bottom rows of Figure 3. In these cases, the perpendicular distortion of the macrocycle is not as evident, but there is a distinct compression parallel to the Cu rows when compared to the porphyrin adsorbed without C−Cu−C bonds. Moreover, the macrocycle in the type $(\mathbf{3/2off})_{2D}$ coupling also rotates by 2.5° and is the most stable predicted structure for the self-assembly of the full 2D overlayer, according to our GGA calculations.

We can now understand why the observed porphyrin structures are all one-dimensional: whereas the binding energies in Figure 2 show that there is a small chemical driving force toward self-assembly in both directions, the energy cost of distorting the porphyrin core and of moving adatoms prevents the porphyrins from coupling in all available directions. This distortion also affects the bonding between macrocycle and surface, which loses some of the hybridization between the π-system of the macrocycle and the sp and d-bands of the substrate. The directionality of the

coupled porphyrin chains is, therefore, governed by mechanical stress in the macrocycles. Note that the mismatch between the repeat lengths in the ⟨110⟩ and ⟨001⟩ surface directions (three and four lattice spacings, respectively) is relatively small and only amounts to 6%. Given that the porphyrin core is quite flexible in the gas phase, it is surprising that this relatively small mismatch has such a large effect on the self-assembly process. We would like to stress that the geometrical analysis discussed in this section is critical for the understanding of our experimental observations.

Fused Porphyrin Chains. Given the apparent lack of self-assembly along the Cu(110) rows due to the lattice mismatch in that direction, the only remaining stepping stone toward two-dimensional self-assembly might be provided by coalescence of porphyrin chains that are already located close together. In fact, as shown in Figure 1 we do see such chains occasionally when annealing the systems at temperatures around 400 °C. These fused-chain structures are illustrated in Figure 4.

The porphyrin cores are very well resolved in the STM images of Figure 4a,b, along with bright protrusions along their outer perimeter which correspond to the coupling Cu atoms. By measuring the distances d_1 to d_7 indicated in Figure 4c from calibrated STM data and comparing them with the periodic repeat lengths in the two lattice directions, it is possible to distinguish three different types of couplings in these coalesced annealed chains: (i) triple C−Cu−C couplings in the ⟨001⟩-direction, corresponding to the energetically most favorable configuration parallel to the Cu rows, Figure 4a,b. (ii) The macrocycles in Figure 4a are coupled with two protrusions in the ⟨110⟩ direction. The triangle formed by the distances d_3, d_4, and d_5 suggests that the two parallel chains are offset by one single row but also that they are otherwise commensurate with the surface. (iii) A third type of coupling is observed in Figure 4b, where the two parallel chains are coupled with three protrusions in the ⟨110⟩ direction, which is consistent with one additional adatom per Cu row covered by the macrocycle. In repeated experiments involving fused chain structures, case ii is observed almost exclusively (at least 98% of parallel couplings), while there are only very few instances of case iii.

We performed large-scale DFT calculations on the two different parallel porphyrin chains that were observed when annealing at up to 400 °C. We model these two double-row structures with a 9 × 3 surface cell containing two adsorbed porphyrin molecules per supercell. The resulting structures along with simulated STM images are shown in Figure 5. As with the full 2D overlayer, we restricted the analysis to the type **3** coupling in the ⟨001⟩-direction, but considered the two experimentally observed couplings of types **2off** and **3** in the perpendicular direction, which we label (**3/2off**)$_{\|}$ and (**3/3**)$_{\|}$. To differentiate our notation from the full

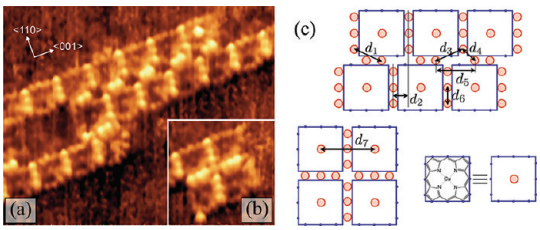

Figure 4. STM images of double-row structures observed when annealing at 400 °C. (a) The most common coupling type between the rows appears to involve two C−Cu−C bonds between each set of adjacent porphyrin rings, which are offset in the ⟨100⟩ surface direction. (b) A rare observation is that the porphyrin rings are not offset in the main growth direction, but are coupled with three Cu-atoms between each of the two chains. (c) Schematic representation of the double-row chains. The labeled distances are measured from the spacings between the Cu adatoms connecting the porphyrin rings. The measured values for the labeled distances are d_1 = 5.7 Å, d_2 = 3.4−3.5 Å, d_3 = 7.8−8.0 Å, d_4 = 3.6−3.7 Å, d_5 = 8.51 Å, d_6 = 2.6 Å, and d_7 = 10.81 Å.

two-dimensional overlayer, "$\|$" is used as a subscript to denote the two parallel coupled chains. The binding energies per porphyrin ring for these structures are obtained as 2.82 and 2.96 eV for the type (**3/2off**)$_{\|}$ and (**3/3**)$_{\|}$ couplings, respectively.

Comparing the calculated binding energies with those in Figure 2 shows that either structure is significantly more stable than the single-row assemblies, but it also predicts the double-row coupling of type (**3/3**)$_{\|}$ in both directions to be the more stable structure by more than 0.1 eV. This prediction is not consistent with our extensive experimental data, which almost exclusively shows inter-row connections of type (**3/2off**)$_{\|}$ with only the rare exceptions being of type (**3/3**)$_{\|}$. From the fully two-dimensional assembly one might also expect that the (**3/2off**)$_{\|}$ coupling provides the most stable intrachain linkage by about 0.5 eV per porphyrin molecule. While detailed analysis in the past has suggested that 0.1 eV is a reasonable lower estimate of the systematic (*e.g.*, functional-dependent) uncertainty in large-scale DFT calculations,[40,41] this particular aspect still leaves an open question about the exact nature of the minimum energy structure. We will return to this problem when discussing the influence of van der Waals interactions.

Figure 5 panels c and d show the STM simulations corresponding to the double row structures discussed in the last paragraph. These images were computed using the same voltage as the experimental images, Figure 5 panels e and f. The very good correspondence between panels (c)↔(e) and (d)↔(f) in Figure 5a,b along with the energetic arguments presented above suggests that the structures shown in Figure 5 represent the experimental observations. In particular, the protrusions corresponding to the coupling perpendicular to the Cu rows are much brighter than those in the parallel direction, in both simulated and experimental

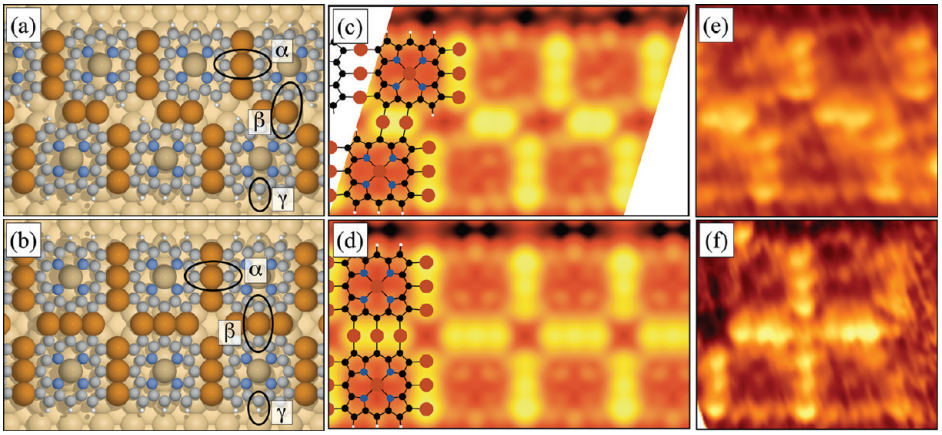

Figure 5. Atomic structure of the double-row porphyrin chains described in the text: (a) for connection type $(3/2c)_{\|}$ with an adsorption energy of E_{ads} = 2.818 eV per macrocycle and (b) for connection type $(3/2c)_{\|}$ with E_{ads} = 2.959 eV per macrocycle. The distances labeled α, β, and γ in these two figures are given in Table 1 and are discussed in the text. (c,d) STM simulations for the two structures in the left panel, using V_{tip} = 0.67 V, which corresponds to the experimental tip voltage. (e,f) Details of the experimental STM images corresponding to the middle panels, taken from Figure 1.

STM images. This is a result of the slightly higher adsorption site taken up for the coupling Cu atoms, which now sit in the much less favorable bridge site rather than in the 4-fold hollow site taken up in the purely one-dimensional Cu−P chain. Our simulations support the idea that the fully annealed structure indeed contains two coalesced porphyrin chains where each macrocycle is held by eight or nine separate, covalent organometallic bonds.

In fact, the different sites occupied by the Cu adatoms involved in the organometallic couplings presented in Figure 5 warrant further discussion, as they provide additional evidence for the role of stress in the molecular arrangement. A number of representative Cu−C distances for the parallel-row structures are labeled in the left panels of Figure 5 and are listed in Table 1. The distances α and β show that the favored Cu−C distance is just below 2 Å, which is almost exactly equal to the sum of the covalent radii of 2.05 Å.[42] However, the distance γ to the next site that should contain an adatom in the case of a fully two-dimensional porphyrin assembly is found to be 28% shorter than the sum of the C and Cu covalent radii. We performed a significant number of different experiments to synthesize an extended 2D layer, but they all stopped with two or three coupled rows, similar to those shown in Figure 5 or with the thermal decomposition of the adsorbate layers.

Influence of van der Waals Interactions. The remaining questions at this point relate to the apparently incorrect energetic ordering predicted for the double-row adsorbate structures presented in Figure 5 and the influence of van der Waals interactions between the surface and adsorbate molecules. At present, the treatment of these interactions is a controversial and debated issue and there is no current consensus on an appropriate method applicable to density functional theory—particularly for the treatment of partially

TABLE 1. C−Cu Distances As Labeled in Figure 5 Panels a and c[a]

coupling type		distance (Å)		
⟨001⟩	⟨110⟩	α	β	γ
3	2off	1.98	1.96	1.47
3	3	1.98	1.96	1.52

[a] Note that the distance type γ labels the horizontal spacing between the C-atom and the next available short-bridge site on top of the Cu rows. For reference, the C and Cu covalent radii are 0.77 Å and 1.28 Å, respectively,[42] which sum to 2.05 Å and give a rough upper estimate of the expected bonding distances.

covalent adsorbate/metal substrate interactions. A back-of-the-envelope estimate for the van der Waals contribution to the physisorption energy of a molecule is at least 80 meV per carbon atom[43,44] and could be as high as 120 meV per carbon atom.[11] For the 20 C-atoms in a porphyrin core, this suggests a dispersive contribution to the surface binding energy of at least 1.6 eV, which is comparable to the covalent bonding energy. One can therefore expect that dispersion interactions do play a significant role in the adsorption process as already discussed by Dyer *et al.*,[36] but it remains to be investigated how influential they are for the energetic hierarchy of different adsorbate structures.

We probe the effect of dispersion forces on the covalent couplings with a variant of the van der Waals density functional developed by Klimeš *et al.*,[45] which uses the nonlocal correlation of the original van der Waals density functional,[46] but with an optimized exchange term. This functional (optB86b-vdwDF) is fitted to a dispersion-dominated reference set of molecular dimers, but it also provides a very good description of measurable parameters for metals. For example, the lattice constant for Cu is equal to 3.60 Å, which is very close to the experimental value of 3.61 Å,[42] and therefore can be expected to provide a very reasonable description

of geometric stress effects that are the core subject of this paper. This particular functional has already been applied successfully to rare-gas adsorption on lead surfaces, where it gives good agreement with available experimental data.[47] A closely related variant of the vdwDF also provided clear evidence that van der Waals effects on a Cu adsorbate can affect the surface/adsorbate interactions, as they are required, for example, to properly describe the wetting of Cu(110).[48] An alternate possibility to introduce dispersive forces into a GGA potential energy landscape would be to include C_6/R^6-style potentials on top of a generalized gradient approximation.[49−51] However, due to the high sensitivity of the computed interaction energies on a necessary *ad hoc* damping function,[52] particularly in the case of metallic substrates, an appropriately chosen van der Waals density functional is the most useful choice at present. In a recent DFT study of single unsubstituted porphyrin molecules adsorbed on a Cu(110) using a vdw-DF,[36] it was found that dispersion forces gave an overall increase of the binding energy by about 40% but did not change the trend of the adsorption energies across different sites. Furthermore, the adsorption geometries changed only slightly.

To assess the effect of van der Waals forces for the Cu-coupled porphyrin chains, we have reoptimized the geometries for most of the coupling configurations presented in Table 2 using the optB86b-vdw density functional discussed above. Self-assembly in the ⟨110⟩ surface direction was not considered, as it was definitely ruled out already by our GGA calculations. The binding energies of all structures that were calculated with both PW91 (GGA) and optB86b-vdw density functionals are presented in Table 2. Compared to GGA, the vdwDF gives an additional binding energy of around 3 eV per porphyrin core for self-assembly in the ⟨001⟩-direction, 2.2−2.6 eV for the hypothetical two-dimensional adlayer, and around 2.7−2.8 eV for the double row chains, which is within the range predicted by our initial back-of-the envelope argument. These results are in agreement with the intuitive idea that more closely bound and less buckled molecules should have a higher dispersion binding energy than the strongly distorted porphyrin cores which are further away from the surface. This is reflected in the adsorption heights and the buckling presented in Table 2. Finally, note that there are only very minor changes of the geometry when including van der Waals interactions.

However, it is worthwhile to compare the details of the energy ordering predicted by the two functionals. We therefore explicitly discuss the hierarchies in Table 2 for the different functionals. Considering the 1D chains perpendicular to the Cu rows, both functionals predict the same energy hierarchy.

1D chains perpendicular to the Cu rows (⟨001⟩ direction):

$$\mathbf{0} > \mathbf{1s} > \mathbf{1as} > \mathbf{2off} > \mathbf{2as} > \mathbf{2s} > \mathbf{3} \qquad (1)$$

TABLE 2. Binding Energies and Adsorption Heights, for Different Self-Assembly (SA) Directions[a]

coupling		binding energy (eV)		adsorption height/buckling (Å)	
⟨001⟩	⟨110⟩	PW91 (GGA)	optB86b-vdwDF	PW91 (GGA)	optB86b-vdwDF
1D SA in the ⟨001⟩ Direction					
0		−1.960	−5.072	2.07/0.34	2.02/0.33
1s		−2.077	−5.106	2.07/0.40	2.04/0.38
1as		−2.258	−5.275	2.07/0.34	2.03/0.37
2s		−2.543	−5.454	2.07/0.49	2.04/0.38
2as		−2.447	−5.400	2.08/0.48	2.05/0.51
2off		−2.400	−5.385	2.09/0.43	2.04/0.43
3		−2.775	−5.631	2.09/0.49	2.06/0.52
2D SA in ⟨001⟩ and ⟨110⟩ Directions					
3	**1s**	−1.800	−4.369	2.07/0.58	2.07/0.58
3	**1as**	−1.605	−4.228	2.08/0.84	2.07/0.84
3	**2s**	−1.193	−3.453	2.08/0.52	2.06/0.58
3	**2as**	−1.677	−4.060	2.06/0.70	2.05/0.70
3	**2off**	−2.319	−4.948	2.04/0.44	2.02/0.45
3	**3**	−1.621	−3.846	2.06/0.70	2.06/0.70
1D SA in ⟨001⟩ Direction with Double Porphyrin Rows					
3	**2off**	−2.818	−5.625	2.05/0.52	2.02/0.55
3	**3**	−2.959	−5.683	2.05/0.43	2.02/0.44

[a] The binding energies per macrocycle are given for PW91 and optB86b-vdw density functionals. The adsorption height is the average height of the C and N atoms above the surface, while the buckling refers to the maximal height difference between any two C and N atoms in each porpyrin core.

For example, **3** is the lowest energy structure (see Scheme 1 and Figure 2). This order is in agreement with the detailed experimental observations of Haq *et al.*[31] Equation 1 verifies that the main energetic ordering leading to the covalent C−Cu−C bonds in the ⟨001⟩ direction is completely unaffected by dispersion interactions, which lends additional credibility to this result.

In the case of the 2D adlayer, the results from the vdW-DF changes the energy hierarchy obtained from Table 2 using the GGA as

$$\text{2D adlayer (GGA)} : (\mathbf{3}/\mathbf{2s})_{2D} > (\mathbf{3}/\mathbf{1as})_{2D} > (\mathbf{3}/\mathbf{3})_{2D} > (\mathbf{3}/\mathbf{2as})_{2D} > (\mathbf{3}/\mathbf{1s})_{2D} > (\mathbf{3}/\mathbf{2off})_{2D}$$

$$\text{2D adlayer (vdwDF)} : (\mathbf{3}/\mathbf{2s})_{2D} > (\mathbf{3}/\mathbf{3})_{2D} > (\mathbf{3}/\mathbf{2as})_{2D} > (\mathbf{3}/\mathbf{1as})_{2D} > (\mathbf{3}/\mathbf{1s})_{2D} > (\mathbf{3}/\mathbf{2off})_{2D} \qquad (2)$$

Given that such an extended layer has not been observed experimentally due to its much higher energy cost than the other structures, it is difficult to assess the ordering in eq 2. The qualitative arguments provided with Figure 3 suggest that the structure $(\mathbf{3/2off})_{2D}$ should be the most favorable structure, given that its porphyrin cores are the least distorted due to their ability to rotate on the Cu(110) surface. The remainder of the hierarchy in eq 2 is due to a mixture of gaining energy by forming additional C−Cu−C organometallic bonds, and losing energy through distortion

of the molecular core which necessarily reduces the overlap between porphyrin and surface electronic states.

The situation is slightly different for the double row chains, where we again have detailed experimental information: At high temperatures, single chains fuse into double rows, which almost exclusively form in the structure (**3/2off**)$_{\|}$ with only the rare exception in structure (**3/3**)$_{\|}$. An overall comparison of the four lowest energy configurations across Table 2 gives the following ordering:

$$\begin{aligned} &\text{most stable (GGA)} : \mathbf{2s} > \mathbf{3} > (\mathbf{3/2off})_{\|} > (\mathbf{3/3})_{\|} \\ &\text{most stable (vdwDF)} : \mathbf{2s} > (\mathbf{3/2off})_{\|} > \mathbf{3} > (\mathbf{3/3})_{\|} \end{aligned} \quad (3)$$

The (**3/3**)$_{\|}$ structure is always found to be most stable in our calculations, but the experimentally observed (**3/2off**)$_{\|}$ porphyrin assembly is calculated to be slightly less favored. In the case of the optB86b-vdwDF, it is only less stable than the lower temperature single row assembly of type **3** by a mere 6 meV. In this context it is again important to note that we are very confident about the structural identification of (**3/2off**)$_{\|}$ using the comparison between the calculated and measured STM images presented in Figure 5.

At present, the physical origins of this discrepancy remain unclear. Several reasons could be responsible for the apparent difference between the experimental and theoretical results, particularly those for the vdwDF. First, our density functional calculations are currently restricted to a few hundred atoms and, therefore, would not take into account any long-range substrate-mediated interactions between neighboring porphyrin molecules, or even neighboring chains. These interactions can easily exceed the small energetic differences found here. Second, the self-assembly of the Cu−porphyrin chains occurs at 400 °C, where vibrational free energies and assembly kinetics could play a significant role. Fully accounting for those effects from first principles is well beyond the reach of computational resources available at present. Finally, we would like to point out that the energy hierarchy of the most stable configurations is based on energy differences that are as small as 6 meV (or about 0.1 meV per adsorbate atom). This is just within the very limit of the currently achievable numerical precision of most density functional calculations for the system size considered here, independent of the systematic accuracy of our density functional methods.

CONCLUSION

This work presents a detailed theoretical and experimental analysis of the covalent self-assembly process recently observed for porphyrin molecules on Cu(110).[31] The main point of interest is that the final annealed structures were not only highly ordered, but they form one-dimensional chains on the surface only in the direction perpendicular to the Cu rows . By considering the energetics of different assembly types and by analyzing the geometries of the computed molecular structures, we find that the commensurability of the adsorbate with the surface plays the main role in determining the structure of the porphyrin chains. During the annealing process, several different porphyrin−porphyrin couplings occur with increasing numbers of connecting Cu adatoms. The result of annealing at 375 °C is an assembly of highly ordered, one-dimensional Cu−porphyrin chains. In a second annealing step, at slightly higher temperatures up to 400 °C, up to two porphyrin chains can fuse together to form a double row.

Using density functional theory, we confirm the mechanism and structure of the observed nanostructures. The generalized-gradient approximation predicts that the fused double-rows are actually the most stable adsorbate structure. This phenomenon is explained using the concept of stress induced in the adsorbate by the self-assembly: while strong chemical driving forces exist to form organometallic C−Cu−C couplings in almost any direction, only the ⟨001⟩ direction actually provides the proper lattice spacings that enable the molecule to fit without significant distortion. This result highlights the critical role of the Cu(110) surface structure in directing assembly and provides an avenue to surface engineering.

Finally, the effect of van der Waals interactions was considered for the Cu−porphyrin assemblies. It was found that the overall prediction of the C−Cu−C coupling and the trend toward multiple organometallic bonds is the same with or without van der Waals interactions. However, the energetic difference of the two candidate structures for the double rows is improved slightly toward the experimentally observed form. Our results suggest that dispersion forces can play an important role even in the assembly of chemisorbed systems where they were not previously regarded to be very significant.

Covalent C−Cu−C couplings of the type described here have been observed in a few distinct systems.[31,30,53] However, this work shows that carbon−copper organometallic bonds on a Cu substrate can be formed as long as the Cu adatoms can sit in energetically favorable surface sites. Moreover, the synthesis recipe can be as simple as *heat-to-connect*, without specific functionalization of any of the adsorbate molecules involved. Due to this apparent simplicity, the C−Cu−C couplings may well rise to one of the standard tools for engineering the self-assembly of nanostructures on surfaces.

METHODS

Periodic density functional calculations were carried out using the VASP computational package[37] with a projector augmented plane-wave basis set.[38] The generalized gradient approximation (GGA) with the PW91 functional was used,[39] as was a variant of the van der Waals density functional[46] where the exchange

term has been replaced by an optimized form of the Becke 86 exchange functional.[45] Throughout this study we used a plane wave energy cutoff of 400 eV, which is sufficient to converge the total energies to within a few meV for this system. This was tested explicitly with a 600 eV cutoff for the adsorbed uncoupled porphyrin molecule. All geometries are relaxed until the maximal force on each atom was less than 0.01 eV/Å.

The Cu(110) surface was described with different supercell sizes according to the direction of self-assembly (SA). All cells contain four Cu layers, with the bottom two layers fixed. The cell sizes used were 6×3 (72 slab atoms, for SA in ⟨001⟩ direction), 4×5 (80 slab atoms, for SA in ⟨110⟩ direction), 4×3 (48 slab atoms, for SA in ⟨001⟩ and ⟨110⟩ directions), and 9×3 (108 slab atoms, for the double-row SA). The Brillouin zone sampling was performed using Monkhorst-Pack[54] grids, chosen such that the length of the lattice vector multiplied with the number of *k*-points in that direction always exceeds 40 Å. Scanning tunneling images were calculated using the Tersoff–Hamann approximation[55] as implemented by Lorente and Persson.[56] The binding energy for each configuration was calculated using single adsorbed H-atoms and single adsorbed Cu atoms as a reference, along with the slab and the Cu–Porphyrin in vacuum:

$$E_{\text{bind}} = E_{\text{configuration}} - E_{\text{substrate}} - E_{\text{Cu - P, vacuum}} - n_{\text{Cu}}E_{\text{Cu, ads}} + 2n_{\text{Cu}}E_{\text{H, ads}} \quad (4)$$

where n_{Cu} is the total number of Cu adatoms, and the total energies of the adsorbed H and Cu atoms are $E_{\text{H,ads}} = E_{\text{substrate+H}} - E_{\text{substrate}}$ and $E_{\text{Cu,ads}} = E_{\text{substrate+Cu}} - E_{\text{substrate}}$, respectively. The Cu adatom reference energy was obtained from the 4-fold hollow site, while the adsorption energy of a single H-atom is obtained from the short-bridge site. These lowest-energy sites were found by comparing the total energy of adsorbed Cu and H atoms on all high-symmetry sites of Cu(110).

STM experiments were performed under UHV conditions using a Specs STM 150 Aarhus instrument. The STM was calibrated to better than 5% accuracy by measuring the atomic distances of the clean Cu(110) surface. All measurements were taken in constant current mode, using a tungsten tip and at a base pressure of 1.5×10^{-10} mbar. Bias voltages are measured at the sample. STM images were enhanced for brightness and contrast using the Image SxM program. The Cu(110) surface was prepared using argon ion sputtering and annealing cycles, and atomic flatness and cleanliness were checked by STM and LEED prior to dosing the molecule. H_2-porphine (Frontier Scientific) was used as purchased and sublimed at ~430 K onto the surface, which was held at room temperature during deposition.

Acknowledgment. We acknowledge computing time provided by the University of Liverpool and by SNAC. Part of this work is financed by the EU project ARTIST (Grant Agreement No. 243421), the UK EPSRC Grant EP/F00981X/1, and the Swedish Natural Science Research Council (VR).

REFERENCES AND NOTES

1. Bartels, L. Tailoring Molecular Layers at Surfaces. *Nat. Chem.* **2010**, *2*, 87.
2. Ciesielski, A.; Palma, C.-A.; Bonini, M.; Samorì, P. Towards Supramolecular Engineering of Functional Nanomaterials: Pre-programming Multi-component 2D Self-Assembly at Solid–Liquid Interfaces. *Adv. Mater.* **2010**, *22*, 3506.
3. Barth, J. V. Fresh Perspectives for Surface Coordination Chemistry. *Surf. Sci.* **2009**, *603*, 1533.
4. Stöhr, M.; Wahl, M.; Spillmann, H.; Gade, L. H.; Jung, T. A. Lateral Manipulation for the Positioning of Molecular Guests within the Confinements of a Highly Stable Self-Assembled Organic Surface Network. *Small* **2007**, *3*, 1336.
5. Madueno, R.; Räisänen, M. T.; Silien, C.; Buck, M. Functionalizing Hydrogen-Bonded Surface Networks with Self-Assembled Monolayers. *Nature* **2008**, *454*, 618.
6. Cheng, Z.; Wyrick, J.; Luo, M.; Sun, D.; Kim, D.; Zhu, Y.; Lu, W.; Kim, K.; Einstein, T. L.; Bartels, L. Adsorbates in a Box: Titration of Substrate Electronic States. *Phys. Rev. Lett.* **2010**, *105*, 066104.
7. Silien, C.; Raäisänen, M. T.; Buck, M. A Supramolecular Network as Sacrificial Mask for the Generation of a Nanopatterned Binary Self-Assembled Monolayer. *Small* **2010**, *3*, 391.
8. Lafferentz, L.; Ample, F.; Yu, H.; Hecht, S.; Joachim, C.; Grill, L. Conductance of a Single Conjugated Polymer as a Continuous Function of its Length. *Science* **2009**, *323*, 1193.
9. Bombis, C.; Ample, F.; Lafferentz, L.; Yu, H.; Hecht, S.; Joachim, C.; Grill, L. Single Molecular Wires Connecting Metallic and Insulating Surface Areas. *Angew. Chem., Int. Ed.* **2009**, *48*, 9966.
10. Cai, J.; Ruffieux, P.; Jaafar, R.; Bieri, M.; Braun, T.; Blankenburg, S.; Muoth, M.; Seitsonen, A. P.; Saleh, M.; Feng, X.; Müllen, K.; Fasel, R. Atomically Precise Bottom-Up Fabrication of Graphene Nanoribbons. *Nature* **2010**, *466*, 470.
11. Björk, J.; Stafström, S.; Hanke, F. Zipping Up: Cooperativity Drives the Synthesis of Graphene Nanoribbons. *J. Am. Chem. Soc.* **2011**, *133*, 14884.
12. Tahara, K.; Furukawa, S.; Uji-i, H.; Uchino, T.; Ichikawa, T.; Zhang, J.; Mamdouh, W.; Sonoda, M.; Schryver, F. C. D.; Feyter, S. D.; Tobe, Y. Two-Dimensional Porous Molecular Networks of Dehydrobenzo[12]annulene Derivatives *via* Alkyl Chain Interdigitation. *J. Am. Chem. Soc.* **2006**, *128*, 16613.
13. Furukawa, S.; Uji-i, H.; Tahara, K.; Ichikawa, T.; Sonoda, M.; Schryver, F. C. D.; Tobe, Y.; Feyter, S. D. Molecular Geometry Directed Kagome and Honeycomb Networks: Toward Two-Dimensional Crystal Engineering. *J. Am. Chem. Soc.* **2006**, *128*, 3502.
14. Lei, S.; Tahara, K.; Schryver, F. C. D.; der Auweraer Y. Tobe, M. V.; Feyter, S. D. One Building Block, Two Different Supramolecular Surface-Confined Patterns: Concentration in Control at the Solid–Liquid Interface. *Angew. Chem., Int. Ed.* **2008**, *47*, 2964.
15. Theobald, J. A.; Oxtoby, N. S.; Phillips, M. A.; Champness, N. R.; Beton, P. H. Controlling Molecular Deposition and Layer Structure with Supramolecular Surface Assemblies. *Nature* **2003**, *424*, 1029.
16. Blunt, M. O.; Russell, J. C.; del Carmen Giminez-Lopez, M.; Garrhan, J. P.; Lin, X.; Schröder, M.; Champess, N. R.; Beton, P. H. Random Tiling and Topological Defects in a Two-Dimensional Molecular Network. *Science* **2008**, *322*, 1077.
17. Elemans, J. A. A. W.; Lei, S.; Feyter, S. D. Molecular and Supramolecular Networks on Surfaces: From Two-Dimensional Crystal Engineering to Reactivity. *Angew. Chem., Int. Ed.* **2009**, *48*, 7298.
18. Ciesielski, A.; Stefankiewicz, A. R.; Hanke, F.; Persson, M.; Lehn, J.; Samorì, P. Rigid Dimers Formed through Strong Interdigitated H-Bonds Yield Compact 1D Supramolecular Helical Polymers. *Small* **2011**, *7*, 342.
19. Grill, L.; Dyer, M.; Lafferentz, L.; Persson, M.; Peters, M. V.; Hecht, S. Nano-architectures by Covalent Assembly of Molecular Building Blocks. *Nat. Nanotechnol.* **2007**, *2*, 687.
20. In't Veld, M.; Iavicoli, P.; Haq, S.; Amabilino, D. B.; Raval, R. Unique Intermolecular Reaction of Simple Porphyrins at a Metal Surface Gives Covalent Nanostructures. *Chem. Commun.* **2008**, 1536–1538.
21. Wegner, D.; Yamachika, R.; Wang, Y.; Brar, V. W.; Bartlett, B. M.; Long, J. R.; Crommie, M. F. Single-Molecule Charge Transfer and Bonding at an Organic/Inorganic Interface: Tetracyanoethylene on Noble Metals. *Nano Lett.* **2008**, *8*, 131.
22. Treier, M.; Pignedoli, C. A.; Laino, T.; Rieger, R.; Müllen, K.; Passerone, D.; Fasel, R. Surface-Assisted Cyclodehydrogenation Provides a Synthetic Route Towards Easily Processable and Chemically Tailored Nanographenes. *Nat. Chem.* **2011**, *3*, 61.
23. Lobo-Checa, J.; Matena, M.; Müller, K.; Dil, J. H.; Meier, F.; Gade, L. H.; Jung, T. A.; Stöhr, M. Band Formation from Coupled Quantum Dots Formed by a Nanoporous Network on a Copper Surface. *Science* **2009**, *325*, 300.
24. Björk, J.; Matena, M.; Dyer, M. S.; Enache, M.; Lobo-Checa, J.; Gade, L. H.; Jung, T. A.; Stöhr, M.; Persson, M. STM Fingerprint of Molecule–Adatom Interactions in a Self-Assembled Metal–Organic Surface Coordination Network on Cu(111). *Phys. Chem. Chem. Phys.* **2010**, *12*, 8815.

25. Matena, M.; Stöhr, M.; Björk, T. R. J.; Martens, S.; Dyer, M. S.; Persson, M.; Lobo-Checa, J.; Enache, K. M. M.; Wadepohl, H.; Zegenhagen, J.; Jung, T. A.; Gade, L. H. Aggregation and Contingent Metal/Surface Reactivity of 1,3,8,10-Tetraazaperopyrene (TAPP) on Cu(111). *Chem.: Eur. J.* **2010**, *16*, 2079.
26. Heim, D.; Écija, D.; Seufert, K.; Auwärter, W.; Aurisicchio, C.; Bonifazi, C. F. D.; Barth, J. V. Self-Assembly of Flexible One-Dimensional Coordination Polymers on Metal Surfaces. *J. Am. Chem. Soc.* **2010**, *132*, 6783.
27. Heim, D.; Seufert, K.; Auwärter, W.; Aurisicchio, C.; Fabbro, C.; Bonifazi, D.; Barth, J. V. Surface-Assisted Assembly of Discrete Porphyrin-Based Cyclic Supramolecules. *Nano Lett.* **2010**, *10*, 122.
28. Liljeroth, P.; Swart, I.; Paavilainen, S.; Repp, J.; Meyer, G. Single-Molecule Synthesis and Characterization of Metal-Ligand Complexes by Low-Temperature STM. *Nano Lett.* **2010**, *10*, 2475.
29. Bedwani, S.; Wegner, D.; Crommie, M. F.; Rochefort, A. Strongly Reshaped Organic−Metal Interfaces: Tetracyanoethylene on Cu(100). *Phys. Rev. Lett.* **2008**, *101*, 216205.
30. Villagómez, C. J.; Sasaki, T.; Tour, J. M.; Grill, L. Bottom-up Assembly of Molecular Wagons on a Surface. *J. Am. Chem. Soc.* **2010**, *132*, 16848.
31. Haq, S.; Hanke, F.; Dyer, M. S.; Persson, M.; Iavicoli, P.; Amabilino, D. B.; Raval, R. Clean Coupling of Unfunctionalized Porphyrins at Surfaces To Give Highly Oriented Organometallic Oligomers. *J. Am. Chem. Soc.* **2011**, *133*, 12031.
32. Liljeroth, P.; Repp, J.; Meyer, G. Current-Induced Hydrogen Tautomerization and Conductance Switching of Naphthalocyanine Molecules. *Science* **2007**, *317*, 1203.
33. Krenner, W.; Klappenberger, F.; Kühne, D.; Diller, K.; Qu, Z. R.; Ruben, M.; Barth, J. V. Positioning of Single Co Atoms Steered by a Self-Assembled Organic Molecular Template. *J. Phys. Chem. Lett.* **2011**, *2*, 1639.
34. Hammer, B.; Nørskov, J. K. Why Gold is the Noblest of all the Metals. *Nature* **1995**, *376*, 238.
35. Donovan, P.; Robin, A.; Dyer, M. S.; Persson, M.; Raval, R. Unexpected Deformations Induced by Surface Interaction and Chiral Self-Assembly of CoII−Tetraphenylporphyrin (Co−TPP) Adsorbed on Cu (110): A Combined STM and Periodic DFT Study. *Chem.—Eur. J.* **2010**, *16*, 11641.
36. Dyer, M. S.; Robin, A.; Haq, S.; Raval, R.; Persson, M.; Klimeš, J. Understanding the Interaction of the Porphyrin Macrocycle to Reactive Metal Substrates: Structure, Bonding, and Adatom Capture. *ACS Nano* **2011**, *5*, 1831.
37. Kresse, G.; Furthmüller, J. Efficient Iterative Schemes for *ab Initio* Total-Energy Calculations Using a Plane-Wave Basis Set. *Phys. Rev. B* **1996**, *54*, 11169.
38. Kresse, G.; Joubert, D. From Ultrasoft Pseudopotentials to the Projector Augmented-Wave Method. *Phys. Rev. B* **1999**, *59*, 1758.
39. Perdew, J. P.; Chevary, J. A.; Vosko, S. H.; Jackson, K. A.; Pederson, M. R.; Singh, D.; Fiolhais, C. Atoms, Molecules, Solids, and Surfaces: Applications of the Generalized Gradient Approximation for Exchange and Correlation. *Phys. Rev. B* **1992**, *46*, 6671.
40. Mortensen, J. J.; Kaasbjerg, K.; Frederiksen, S. L.; Nørskov, J. K.; Sethna, J. P.; Jacobsen, K. W. Bayesian Error Estimation in Density-Functional Theory. *Phys. Rev. Lett.* **2005**, *216401*, 95.
41. Carlsson, J. M.; Hanke, F.; Linic, S.; Scheffler, M. Two-Step Mechanism for Low-Temperature Oxidation of Vacancies in Graphene. *Phys. Rev. Lett.* **2009**, *102*, 166104.
42. Kittel, C. *Introduction to Solid State Physics*, 7th ed.; John Wiley & Sons: New York, 1996; p 78.
43. Björk, J.; Hanke, F.; Palma, C.; Samorì, P.; Cecchini, M.; Persson, M. Adsorption of Aromatic and Anti-Aromatic Systems on Graphene through $\pi-\pi$ Stacking. *J. Phys. Chem. Lett.* **2010**, *1*, 3407.
44. Mura, M.; Gulans, A.; Thonhauser, T.; Kantorovich, L. Role of van der Waals Interaction in Forming Molecule−Metal Junctions: Flat Organic Molecules on the Au (111) Surface. *Phys. Chem. Chem. Phys.* **2010**, *12*, 4759.
45. Klimeš, J.; Bowler, D. R.; Michaelides, A. Van der Waals Density Functionals Applied to Solids. *Phys. Rev. B* **2011**, *83*, 195131.
46. Dion, M.; Rydberg, H.; Schroder, E.; Langreth, D. C.; Lundqvist, B. I. Van der Waals Density Functional for General Geometries. *Phys. Rev. Lett.* **2004**, *92*, 246401.
47. Zhang, Y. N.; Hanke, F.; Bortolani, V.; Persson, M.; Wu, R. Q. Why Sliding Friction of Ne and Kr Monolayers Is So Different on the Pb(111) Surface. *Phys. Rev. Lett.* **2011**, *106*, 236103.
48. Carrasco, J.; Santra, B.; Klimeš, J.; Michaelides, A. To Wet or Not to Wet? Dispersion Forces Tip the Balance for Water Ice on Metals. *Phys. Rev. Lett.* **2011**, *106*, 026101.
49. Grimme, S. Semiempirical GGA-type Density Functional Constructed with a Long-Range Dispersion Correction. *J. Comput. Chem.* **2006**, *27*, 1787–1799.
50. Tkatchenko, A.; Scheffler, M. Accurate Molecular Van Der Waals Interactions from Ground-State Electron Density and Free-Atom Reference Data. *Phys. Rev. Lett.* **2009**, *102*, 73005.
51. Grimme, S.; Antony, J.; Ehrlich, S.; Krieg, H. A Consistent and Accurate *ab Initio* Parametrization of Density Functional Dispersion Correction (DFT-D) for the 94 Elements H-Pu. *J. Chem. Phys.* **2010**, *132*, 154104.
52. Hanke, F. Sensitivity Analysis and Uncertainty Calculation for Dispersion-Corrected Density Functional Theory. *J. Comput. Chem.* **2011**, *32*, 1424.
53. Walch, H.; Gutzler, R.; Sirtl, T.; Eder, G.; Lackinger, M. Material- and Orientation-Dependent Reactivity for Heterogeneously Catalyzed Carbon-Bromine Bond Homolysis. *J. Phys. Chem. C* **2010**, *114*, 12604.
54. Monkhorst, H. J.; Pack, J. D. Special Points for Brillouin-Zone Integrations. *Phys. Rev. B* **1976**, *13*, 5188.
55. Tersoff, J.; Hamann, D. R. Theory of the Scanning Tunneling Microscope. *Phys. Rev. B* **1985**, *31*, 805.
56. Lorente, N.; Persson, M. Theoretical Aspects of Tunneling-Current−Induced Bond Excitation and Breaking at Surfaces. *Faraday Discuss.* **2000**, *117*, 277.